An Efficient Monte Carlo Algorithm for the Fast Equilibration and Atomistic Simulation of Alkanethiol Self-Assembled Monolayers on a Au(111) Substrate

Orestis Alexiadis,[†,‡] Kostas Ch. Daoulas,[§] and Vlasis G. Mavrantzas*[,†,‡]

Institute of Chemical Engineering and High-Temperature Chemical Processes (FORTH-ICE/HT), Patras GR 26504, Greece, University of Patras, Department of Chemical Engineering, Patras GR 26504, Greece, Institut für Theoretische Physik, Georg-August Universität, 37077 Göttingen, Germany

Received: August 9, 2007; In Final Form: October 22, 2007

A new Monte Carlo algorithm is presented for the simulation of atomistically detailed alkanethiol self-assembled monolayers (R−SH) on a Au(111) surface. Built on a set of simpler but also more complex (sometimes nonphysical) moves, the new algorithm is capable of efficiently driving all alkanethiol molecules to the Au(111) surface, thereby leading to full surface coverage, irrespective of the initial setup of the system. This circumvents a significant limitation of previous methods in which the simulations typically started from optimally packed structures on the substrate close to thermal equilibrium. Further, by considering an extended ensemble of configurations each one of which corresponds to a different value of the sulfur−sulfur repulsive core potential, σ_{ss}, and by allowing for configurations to swap between systems characterized by different σ_{ss} values, the new algorithm can adequately simulate model R−SH/Au(111) systems for values of σ_{ss} ranging from 4.25 Å corresponding to the Hautman−Klein molecular model (*J. Chem. Phys.* **1989**, *91*, 4994; **1990**, *93*, 7483) to 4.97 Å corresponding to the Siepmann−McDonald model (*Langmuir* **1993**, *9*, 2351), and practically any chain length. Detailed results are presented quantifying the efficiency and robustness of the new method. Representative simulation data for the dependence of the structural and conformational properties of the formed monolayer on the details of the employed molecular model are reported and discussed; an investigation of the variation of molecular organization and ordering on the Au(111) substrate for three $CH_3-(CH_2)_n-SH$/Au(111) systems with $n = 9$, 15, and 21 is also included.

A. Introduction

Self-assembled monolayers (SAMs) of *n*-alkanethiol molecules, $CH_3-(CH_2)_n-SH$, on a Au(111) surface—also known as R−SH/Au(111) SAMs—serve as a prototypical model for studying chain packing, ordering, binding, and microscopic structure in monomolecular films formed by the spontaneous adsorption of amphifunctional or end-functionalized molecules on a solid surface.[1,2] Given the relative ease of preparation, the high degree of structural ordering achieved, the good adhesion to the substrate, and their good thermal, chemical, and mechanical stability properties, these systems find extensive applications in a variety of fields: in the production of thin films from organic materials, in optics and electronics, as means for controlling the hydrophobic or hydrophilic behavior of a surface, as coatings for the protection of surfaces from corrosion, in molecular recognition, and more recently even as biosensors.[1] This also explains why SAMs and, in particular, the R−SH/Au(111) systems, have been studied so extensively both experimentally and theoretically.[1]

At full coverage phase, the one that corresponds to the highest possible molecular packing, R−SH/Au(111) systems exhibit highly ordered structures not only in the way sulfur atoms are organized onto the Au surface but also in the structure that the chain backbone displays, as depicted in Figure 1. The chains adopt an all-trans configuration, with the backbone structure being characterized by a tilt (θ), a twist (Φ), and a precession

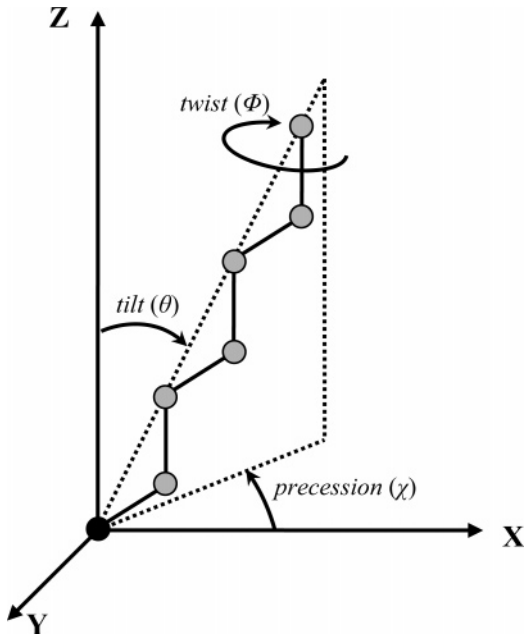

Figure 1. Angles associated with the orientation of an alkanethiol chain, $CH_3(CH_2)_n-SH$, on the Au(111) surface: The tilt angle is defined by the end-to-end vector of the molecule with respect to the *z* coordinate axis, the twist angle corresponds to the rotation of the all-trans plane about the chain end-to-end axis, and the precession angle describes the tilt direction.

* Corresponding author. E-mail: vlasis@chemeng.upatras.gr. Phone: +30-2610-997-398. Fax: +30-2610-965-223.
† Institute of Chemical Engineering and High-Temperature Chemical Processes (FORTH-ICE/HT).
‡ University of Patras.
§ Georg-August Universität.

10.1021/jp076417+ CCC: $40.75
Published on Web 01/09/2008

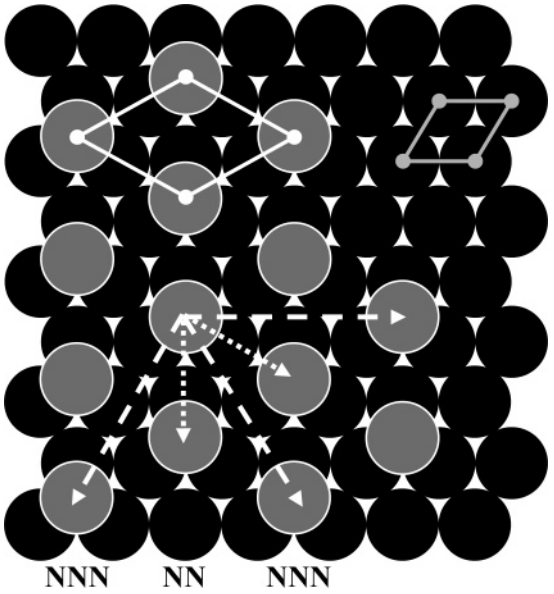

Figure 2. Hexagonal coverage on the Au(111) phase. The black circles represent Au atoms, and the gray circles, sulfur atoms. The white solid lines outline the lattice space of the $(\sqrt{3} \times \sqrt{3})R30°$ ordering, while the gray solid lines define the unit cell of the Au(111) crystallographic plane. The dotted arrows point toward the nearest neighbor (NN) direction, and the dashed ones toward the next nearest neighbor (NNN) direction.

(χ) angle. Several experimental studies have established that R−SH/Au(111) SAMs demonstrate an average tilt angle ranging from 30 to 40°[3−6] with the all-trans backbone plane of the carbon atoms rotated by about 52−55° with respect to the tilt direction plane.[3,4] Earlier diffraction studies of R−SH/Au(111) SAMs showed that these systems adopt a simple hexagonal $(\sqrt{3} \times \sqrt{3})R30°$ overlayer lattice on Au(111), with a lattice spacing of 4.97 ± 0.05 Å and one chain per unit cell.[7−9] Later diffraction (LEAD,[10] GIXD[11]) and ultrahigh vacuum scanning tunneling microscopy (STM)[12,13] measurements, however, indicated that a superlattice structure of the commensurate $(\sqrt{3} \times \sqrt{3})R30°$ unit mesh is present. The observed rectangular unit mesh, of dimensions $(2\sqrt{3} \times 3)$ in units of nearest neighbor distance of substrate, a_{au}, contains four hydrocarbon chains with two nonequivalent chains per unit cell (twist angles that differ by about 90°[4,14] and different adsorption sites of the sulfur atoms on the gold substrate[15,16]) and can also be described as a $c(4 \times 2)$ superlattice of the $(\sqrt{3} \times \sqrt{3})R30°$ lattice. The hexagonal and rectangular structural models are depicted in Figures 2 and 3, respectively.

To understand the structural properties and domain formation of alkanethiol SAMs on the Au(111) surface, molecular dynamics (MD) and Monte Carlo (MC) simulations have also been carried out.[17−27] From the point of view of ab initio simulations, attention has been paid to the investigation of the Au−S interaction and the different adsorption sites on the Au(111) substrate.[28−32] These ab initio calculations paved the way for the development of several force fields for use in atomistic (MC and MD) simulations. Hautman and Klein[17,18] performed MD simulations using the united-atom model for the interactions between CH_3, CH_2, and S pseudoatoms, while the surface was simulated as a continuum interacting with united atoms based on a structureless 12−3 Lennard-Jones (LJ) potential. With the same model but with a different value of the headgroup−headgroup size parameter, σ_{ss} (equal to 4.97 Å instead of 4.25 Å), in order to fix the S−S spacing on the Au(111) substrate to its experimental value, also MC simulations were carried out by Siepmann and McDonald.[19] Later, Mar and Klein[20] using

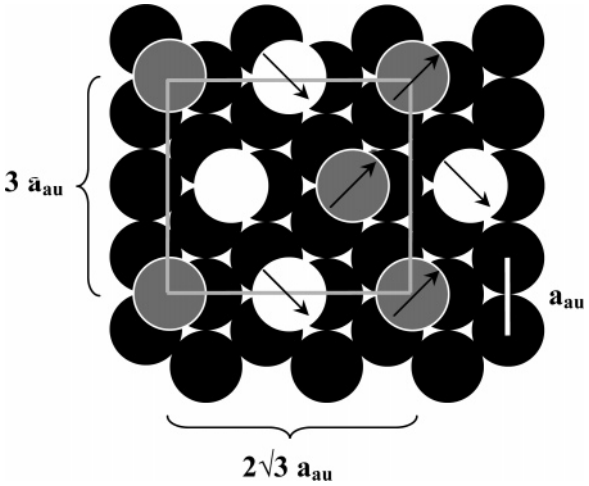

Figure 3. One possible representation of the $c(4 \times 2)$ or $(2\sqrt{3} \times 3)$ structure. Sulfur atoms are represented here with white and gray circles, while the black arrows reflect the projection of the last carbon bond on the gold surface (for clarity, chains are assumed standing normal to the surface) corresponding to the different chain conformations relative to the twist angle.

an alkyl chain model in full atomic detail found out that the stable crystalline structure in their MD simulations was the herringbone two-chain arrangement per unit cell. Bhatia and Garrison[22,23] used a detailed atom description of the Au(111) substrate consisting of eight layers, with the top three layers moving according to Newton's equations and the Au−S interactions being governed by a Morse potential. They proposed four structures of the $c(4 \times 2)$ superlattice, two of them stable only for a short time and the two others stable only at lower temperatures (<100 K). In a recent work, Vamparala et al.[27] performed a large scale MD simulation with an all atom model in order to investigate the structural properties of these monolayers and their dependence on temperature, lattice spacing, and chain length. They manipulated the gold surface in the same manner as Hautman and Klein, but they added an extra term in the 12−3 LJ potential to constrain the motion of sulfur atoms on the $x-y$ plane.

With no exception, in all of these studies, the MC or MD simulations were started from an initial configuration in which the alkanethiols had already been adsorbed on the Au(111) surface to form the characteristic structure of a monolayer film. The sulfur atoms were always assumed to be arranged in the $(\sqrt{3} \times \sqrt{3})R30°$ lattice or $c(4 \times 2)$ superlattice configuration, while the alkane chains were taken to be in the all-trans configuration (with the planes of the backbone carbon atoms in the herringbone arrangement). What was simulated then was structural details and issues related to local dynamics in the monolayer as a function of temperature and molecular length for systems of alkanethiols containing up to 25 carbon atoms per chain. For the MD simulations, in particular, given that the evolution of the system was monitored for times that never exceeded 100 ps (whereas the longest relaxation time of the system can be as high as a few hundred nanoseconds), it is understood that what was really simulated was only short atomic displacements from the positions of the initial configuration, that is, only short-time system fluctuations around the assumed initial configuration.

To address the issue of the generation of a fully equilibrated initial configuration and, simultaneously, overcome problems associated with the long relaxation times exhibited by systems of chain molecules (such as the R−SH/Au(111) SAMs) in atomistic MD simulations, we propose here a new simulation

methodology: (a) No assumption is made about the structure of the formed monolayer for the given molecular model (forcefield). Instead, the monolayer is gradually formed in the simulation starting from a bulk system configuration, thanks to the design and implementation of a novel MC algorithm that can run either serially or in parallel and is capable of driving sulfur atoms to the Au(111) substrate within modest computation time. (b) The structural properties of the formed monolayer are calculated as ensemble averages over a large number of fully equilibrated system configurations accumulated in the course of the MC simulation once the formation of the film has been completed. Extra information about the dynamic properties of the monolayer can be extracted in a third stage, by borrowing a system configuration, fully pre-equilibrated with the new MC algorithm, and subjecting it to a long MD simulation with a multiple time step (MTS) algorithm, allowing one to track system evolution for times on the order of hundreds of nanoseconds up to microseconds.

The new simulation method is based on the implementation of a number of clever (in some cases, even nonphysical or fictitious) MC moves tailored to enhance the efficiency of configurational sampling. Starting from an initial configuration of randomly distributed chains of alkanethiols in space with their number density chosen so as to correspond to full surface coverage once the state of thermodynamic equilibrium has been reached, the new simulation method is so robust that it can efficiently drive all S atoms to the Au(111) substrate, thereby avoiding the need to start the simulation from an initial configuration that is close to the final system structure.

It should be noted here that the difficulty of forming a monolayer film with a 100% surface coverage is not merely a computational problem. Experimental studies have shown that the rate of formation of a SAM is influenced by many factors, such as temperature, chain length, cleanliness of the surface, rate of reaction with the surface, and reversibility of adsorption.[16] In the case of monolayers formed by the spontaneous assembly of organic thiols onto gold, one observes an initial, rapid adsorption followed by a slower period during which the thickness slowly approaches its final value. The rapid adsorption results in an imperfect monolayer, while in the following slower period additional adsorption takes place (involving possibly lateral diffusion on the surface) which reduces defects and enhances packing.[16]

The paper is organized as follows: Section B discusses the molecular model employed in the atomistic MC simulations of this work. A detailed description of all MC moves implemented in the simulations is given in section C. Section D discusses the simulation methodology and presents results for three $CH_3-(CH_2)_n-SH/Au(111)$ systems with $n = 9$, 15, and 21, respectively, validating and evaluating the efficiency of the new algorithm. Representative results about the structure and conformation of the monolayers formed by the adsorption of these three alkanethiol systems on Au(111), as obtained from the new simulation algorithm, are presented in section E. The first set of results refers to the $CH_3-(CH_2)_9-SH/Au(111)$ system and the comparison between the two molecular models employed in the MC simulations. The second set refers to the dependence of the structure and conformation of the monolayers formed on chain length, as obtained with the molecular model of Hautman and Klein.[17] The paper concludes with section F discussing the major findings of the present work.

B. Molecular Model: Interaction Potentials

Two different molecular models were employed in the MC simulations of the present study. The first (model I), proposed by Hautman and Klein,[17,18] distinguishes between methyl (CH_3), methylene (CH_2), and sulfur (S) groups or atoms along an R−SH molecule, each of which is regarded as a different Lennard-Jones (LJ) interaction site. In the Hautman−Klein model,

(i) All C−C and S−C bond lengths are held fixed, equal to 1.53 and 1.82 Å, respectively.

(ii) Bond angle fluctuations are described by a harmonic potential function of the form

$$U_b(\theta) = \frac{1}{2} k_\theta (\theta - \theta_0)^2 \tag{1}$$

with k_θ and θ_0 values borrowed from the calculations of Jorgensen[33] for the development of potential functions for liquid thiols; they are summarized in Table 1.

(iii) Dihedral angles are governed by the Ryckaert−Bellemans torsional potential[34]

$$U_t(\phi) = \sum_{i=0}^{5} a_i \cos^i(\phi) \tag{2}$$

with the values of the coefficients, α_i, reported in Table 2.

(iv) A 12−6 LJ potential describes all nonbonded interactions (intermolecular and intramolecular ones for all atom pairs separated by more than three bonds):

$$U_{LJ}(r_{ij}) = \begin{Bmatrix} 4\epsilon_{ij}\left[\left(\frac{\sigma_{ij}}{r_{ij}}\right)^{12} - \left(\frac{\sigma_{ij}}{r_{ij}}\right)^{6}\right] & r_{ij} \le r_c \\ 0 & r_{ij} > r_c \end{Bmatrix} \tag{3}$$

where i and j represent the three types of atomistic units and r_c is the cutoff distance (12 Å in the present work). The values of constants σ_{ij} and ϵ_{ij} are summarized in Table 3; standard Lorentz−Berthelot mixing rules of the form

TABLE 1: Harmonic Potential Function Parameters (Taken from ref 17) Governing Bond Angle Fluctuations

parameter	C−C−C	S−C−C
k_θ (kcal mol^{-1} rad^{-2})	124.2	124.2
θ_0 (deg)	109.5	114.4

TABLE 2: Values of the Coefficients, α_i, of the Ryckaert−Bellemans Torsional Potential (Taken from ref 17) Governing Dihedral Angles

parameter	X−C−C−C (kcal/mol); X = S, C
α_0	2.217
α_1	2.905
α_2	−3.135
α_3	−0.731
α_4	6.271
α_5	−7.527

TABLE 3: Values of the Lennard-Jones Potential Parameters (Taken from ref 17) Describing Intramolecular and Intermolecular Interactions

interaction pair	σ (Å)	ϵ (kcal mol^{-1})
CH_3-CH_3	3.905	0.1751
CH_2-CH_2	3.905	0.118
S−S	4.25−4.97	0.3974
CH_3-CH_2[a]	3.905	0.1437
CH_3-S[a]	3.7275	0.2094
CH_2-S[a]	3.7275	0.1719

[a] Parameters calculated with the Lorentz−Berthelot rule (eq 4 in the main text).

$$\sigma_{ij} = \frac{1}{2}(\sigma_i + \sigma_j), \quad \epsilon_{ij} = \sqrt{\epsilon_i \epsilon_j} \tag{4}$$

can then be used to describe cross interactions wherever the parameters σ_{ij} and ϵ_{ij} are not available.

(iv) Also, as far as the interactions of sulfur and carbon atoms with the gold surface are concerned, these are modeled by a 12−3 LJ potential, which is a function only of the perpendicular (z) distance from the gold substrate:

$$U_{\text{surf}} = \frac{C_{12}}{(z - z_0)^{12}} - \frac{C_3}{(z - z_0)^3} \tag{5}$$

where z denotes the distance of the pseudoatom from the Au(111) basal plane and z_0, C_3, and C_{12} are numerical constants with values as listed in Table 4.

The second molecular model (model II) was proposed by Siepmann and McDonald[19] and also distinguishes between methyl (CH_3), methylene (CH_2), and sulfur (S) groups or atoms along an R−SH molecule, each of which is regarded as a different LJ interaction site. Compared to the Hautman−Klein model, however, a significantly larger value for the headgroup−headgroup (S−S) size parameter, σ_{ss} (equal to 4.97 Å as compared to 4.25 Å), is assumed for the corresponding LJ potential in order to fix the S−S spacing on the Au substrate to its experimental value.

The most important disadvantage of models I and II employed here is that they do not take into account the atomistic detail and structure of the Au(111) substrate; a rather smooth surface potential is assumed so that the interaction of all pseudoatoms along an alkanethiol molecule with the substrate is a function only of the perpendicular (z) distance from the gold surface. Other models of surface potentials[23,31] employ a more accurate description of the substrate by explicitly taking into consideration gold atoms at their correct crystallographic positions along the (111) plane. The structures predicted from these more detailed models are reported to be closer to the $c(4 \times 2)$ superlattice structure at ambient temperatures which is usually the experimentally observed structure.

C. Monte Carlo Moves

As already mentioned above, key to the success of the proposed methodology is a novel MC algorithm based on a combination of simple and more complex moves (sometimes nonphysical) which increase the efficiency with which phase space is sampled, thereby resulting in equilibration rates that are orders of magnitude faster than those achieved by known dynamic methods (such as atomistic MD). In the recent past, some of these moves have been successfully implemented in simulating a variety of chain systems, including bulk melts of long-chain linear and nonlinear (branched) polyethylene, linear polydienes (*cis*-1,4-polyisoprene and *cis*-1,4-polybutadiene), linear polyethylene melts adsorbed on a graphite basal plane, and terminally grafted chains on a hard wall.[35−39] Here, they have been redesigned so as to be applicable for the specific architecture of the simulated $CH_3-(CH_2)_n-SH$/Au(111) systems. Unfortunately, to keep the simulated systems strictly monodisperse, some very efficient moves (such as the end-bridging[36] and the generalized reptation[37−41]), which effect changes in the polydispersity of the system, had to be disregarded. To keep the cocktail of applied moves robust and to ensure an ergodic simulation, however, two new MC moves are introduced here, the atom-identity exchange and the bias reptation. A detailed description of all moves employed in the simulations of this work is presented in the next paragraphs of this section.

TABLE 4: Values of the C_3, C_{12}, and z_0 Constants of the 12−3 Lennard-Jones Potential (Taken from ref 17) Describing the Interactions of the United Atoms along an Alkanethiol Chain with the Au(111) Substrate

united atom	C_{12} (10^4 kcal Å^{12} mol^{-1})	C_3 (kcal Å^3 mol^{-1})	z_0 (Å)
CH_3	6.776	41.33	0.86
CH_2	5.564	33.98	0.86
S	8.126	358.89	0.269

1. Simple Monte Carlo Moves. *Flip.* This move involves a rotation of a randomly selected internal atom along an alkanethiol chain about the axis connecting the atoms on the left and the right of the selected mer. The rotation involves randomly altering the pertinent torsional angle by a value which is randomly picked from a uniform distribution in the interval (−30°, 30°); the position of the rotating atom is then computed according to the specified bond lengths. As a result, the values of two bending and four torsional angles (at most) are changed in a flip move, while all bond lengths remain unaltered. Some extra care should be taken when the second atom along the $CH_3-(CH_2)_n-SH$ chain (right next to the sulfur atom) is selected for rotation due to the different value of the S−C bond length from the rest of the C−C bond lengths; in this case, the geometric solution of the flip move should be slightly modified.

End Rotation. This move proceeds by rotating a randomly selected chain-end atom about the axis of the bond prior to the last one along the alkanethiol chain; the corresponding dihedral angle is uniformly selected in the interval (−180°, 180°). The bending angle of the last bond is also altered; here, it is chosen on the basis of a probability distribution which is proportional to $\exp(-(k_\theta/2k_BT)(\theta - \theta_0)^2)\sin\theta$, where k_B denotes the Boltzmann constant. This allows expressing the acceptance criterion simply as

$$p_{\text{acc}} = \min\left[1, \exp\left(-\frac{\Delta E}{K_B T}\right)\right] \tag{6}$$

where ΔE denotes the potential energy difference between the states after and before the implementation of the move without taking into account the bond bending contribution.

Configurational Bias. Configurational bias (CB) is based on the ideas of Rosenbluth−Rosenbluth[42] for the simulation of self-avoiding walks in lattice polymer models. Its application to polymer systems in phase space, as it has been presented by de Pablo et al.,[43] Siepmann and Frenkel,[44] and Leontidis et al.,[45] involves three steps:

(1) First, an alkanethiol chain is picked and a random number of its monomers, N_{cut}, are cut at either end of the chain. The size of N_{cut} has a crucial effect on the acceptance rate of the move;[46] here, its value has been chosen to range from 1 to 6.

(2) Next, a step-by-step regeneration of the extracted segment is attempted in a biased fashion, in which a number, N_{dis}, of prospective positions (four in this work) is selected for the reproduction of every single atom in the excised segment, as schematically illustrated in Figure 4a. The selection of the torsion and bond bending angles of every trial position, which is based on the Boltzmann factor of the sum of the torsional and bond bending potentials, is followed by the calculation of the total system energy (involving the sum of the potential energy changes effected in the intramolecular and intermolecular LJ interactions plus surface contributions). The selection of the new position is based on the following probability:

$$P_i = \frac{w_i}{\sum_{j=1}^{N_{\text{dis}}} w_j} \tag{7}$$

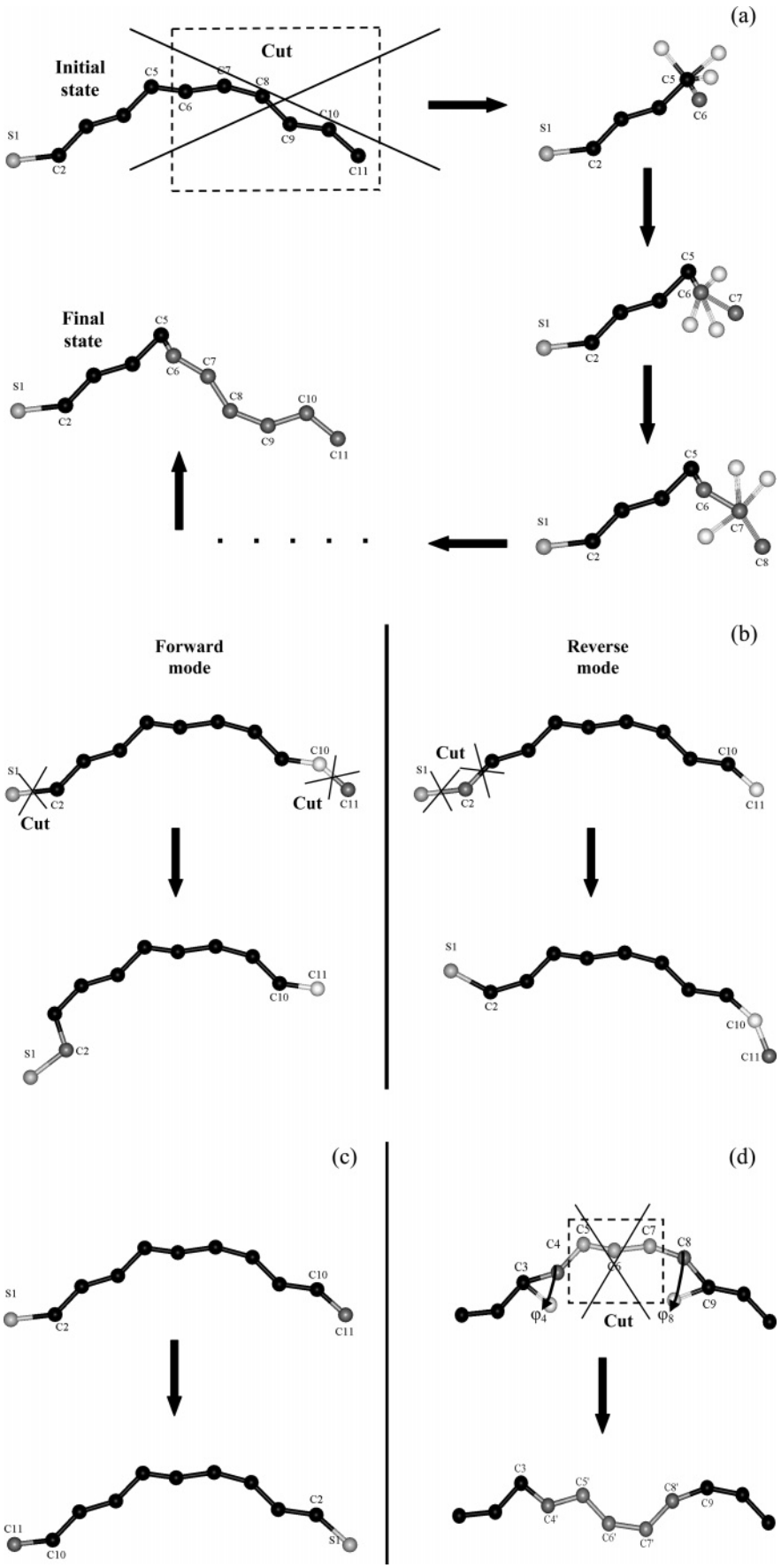

Figure 4. Schematic representation of some of the simpler MC moves employed in the present simulations: (a) configurational bias; (b) modified bias reptation (forward and reverse); (c) atom-identity exchange; (d) concerted rotation.

where

$$w_j = \exp\left(-\frac{U_j}{K_B T}\right) \tag{8}$$

with U_j denoting the sum of the energy contributions from the LJ and surface interactions. This process, which is repeated N_{cut} times so that a full trial configuration of the chain is created, comprises an illustrative example of a configurational biased system selection.

(3) The method proceeds by applying the correct form of the acceptance criterion, which removes the bias introduced in the selection process. Namely, in the new chain pattern, a Rosenbluth statistical weight of the form

$$W^{\text{old}\rightarrow\text{new}} = \prod_{i=1}^{N_{cut}} P_i \tag{9}$$

corresponds. $W^{\text{new}\rightarrow\text{old}}$ is given from the solution of the reverse problem so that the equation that determines the acceptance of the move is finally written as[43]

$$p_{acc} = \min\left[1, \frac{W^{\text{new}\rightarrow\text{old}} \exp\left[-\frac{(U_{LJ}^{new} + U_{surf}^{new})}{K_B T}\right]}{W^{\text{old}\rightarrow\text{new}} \exp\left[-\frac{(U_{LJ}^{old} + U_{surf}^{old})}{K_B T}\right]}\right] \tag{10}$$

Here, $(U_{LJ}^{new} + U_{surf}^{new})$ and $(U_{LJ}^{old} + U_{surf}^{old})$ are the system energy contributions from the LJ and surface interactions in the new and old configuration, respectively.

The configurational bias (CB) move, along with the generalized reptation and end rotation moves, is very important when adsorbed systems are simulated, because it guarantees the mobility of free ends not only in the bulk but also near the substrate; this is clearly the case also for the R−SH/Au(111) systems studied here.

Modified Bias Reptation. The conventional reptation move involves cutting off an atom at either end of a chain and appending it to the other end by choosing new bending and dihedral angles. For the case of the simulated alkanethiol molecules containing a sulfur atom at one of their ends, the reptation move is modified as follows: First, the end monomers (S and CH_3) in a randomly selected chain are extracted and the CH_3 pseudoatom is rebuilt in place of the S atom. The type of CH_3 in the atomistic unit is then changed to CH_2, and a S atom is regenerated over the new CH_2 monomer. The modified reptation move is schematically depicted in Figure 4b. In order to increase the performance of the move, reptation is realized in a biased fashion using appropriately defined Boltzmann factors so that overlaps with surrounding atoms in the same or neighboring chains are avoided. The method proceeds in the same manner as the configurational bias move. The implementation of the reverse reptation move is also crucial so as to ensure microscopic reversibility.

Atom-Identity Exchange. This move is introduced in order to accelerate the adsorption of chains onto the Au(111) surface. Atom-identity exchange consists of swapping the types between the head (S) and the terminal (CH_3) groups in a randomly selected alkanethiol chain while simultaneously altering the direction of the chain backbone, as Figure 4c shows. In practice, the move is implemented through an "elongation" of the CH_2-CH_3 bond from 1.53 to 1.82 Å and a "reduction" of the $S-CH_2$ bond to 1.53 Å without changing the relevant bending and torsional angles.

Concerted Rotation. The concerted rotation (CONROT) move, which was developed initially by Dodd et al.[47] for the simulation of polymer melts and glasses and generalized later by Pant and Theodorou,[36] was designed in order to effect significant local rearrangements not only in the ends but also in the interior of the chains. The move is initiated by removing a trimer of consecutive atoms in the chain and driving the two atoms neighboring the trimer by effecting a change in the torsion angle by a value which is randomly chosen within prespecified bounds $(-\delta\varphi_{max}, \delta\varphi_{max})$. As shown schematically in Figure 4d, given the new coordinates of the two driven atoms (*C4*, *C8*), the geometric problem of trimer bridging is invoked[36,38] according to which an appropriate conformation of the trimer (*C5*−*C6*−*C7*) is sought so as to connect the two dimers (*C3*−*C4*) and (*C8*−*C9*) in such a way that the bonds of the altered segment (*C3*−*C4′*−*C5′*−*C6′*−*C7′*−*C8′*−*C9*) preserve their equilibrium lengths (1.53 and 1.82 Å for C−C and S−C bonds, respectively) given predefined values for all bending angles involved in the move.

2. More Complex Monte Carlo Moves. The moves discussed in section C.1 permit complete equilibration (within reasonable CPU time) of relatively short $CH_3-(CH_2)_n-SH$/Au(111) systems, that is, for *n* values less than about 15. For higher *n* values, it is generally observed that, although these moves do reliably sample local density and energy fluctuations in the monolayer, they are not robust enough for driving all alkanethiol molecules to the Au(111) plane to lead to 100% surface coverage. Guided by strategies followed to overcome similar problems in simulations of long-chain bulk homopolymers, three additional and more complex moves were redesigned and implemented here for the simulation of longer $CH_3-(CH_2)_n-SH$/Au(111) systems: double-bridging (DB), intramolecular double-rebridging (IDR), and self-end-bridging (SEB). These moves induce alterations in the connectivity of the simulated chains, and their formulation for the simulated $CH_3-(CH_2)_n-SH$/Au(111) SAMs is discussed in the next paragraphs of this section.

Double-Bridging Moves (DB and IDR). The DB and IDR double-bridging moves constitute a generalization of the end-bridging (EB) move, and they were designed[48,49] to deal with two constraints associated with its use: its inability to simulate strictly monodisperse systems of oligomers and polymers and the strong dependence of its efficiency on the presence of chain ends and chain orientation. These moves are based on the formation of two bridging trimers between four properly chosen atoms along two selected system chains. A schematic illustration of the DB move before and after acceptance is presented in Figure 5a. The move is realized by selecting an internal atom *Ap* of chain (A) involved in the primary bridging with atom *Bp* of chain (B). In detail, a trimer of consecutive atoms adjacent to atom *Bp*, namely (*B1*−*B2*−*B3*), is being removed and the primary bridging between atoms *Ap* and *Bp* takes place by constructing a new trimer (*B1′*−*B2′*−*B3′*). The move is completed with a secondary bridging between atom *Bs* lying next to the excised trimer (*B1*−*B2*−*B3*) of chain (B) and atom *As* of chain (A). This is implemented by extracting the trimer (*A1*−*A2*−*A3*) connecting atoms *Ap* and *As* of chain (A) and by forming a new trimer (*A1′*−*A2′*−*A3′*) to bridge atom *As* with atom *Bs*. As can be seen in Figure 5a, upon acceptance, the conformations of chains corresponding to (A′) and (B′) are dramatically altered compared to those of (A) and (B). Given the initial configuration, the DB move can result in a maximum of four different configurations from which only one maintains monodispersity (the one depicted in Figure 5a). Due to the fact that the systems under study in this work must be kept strictly

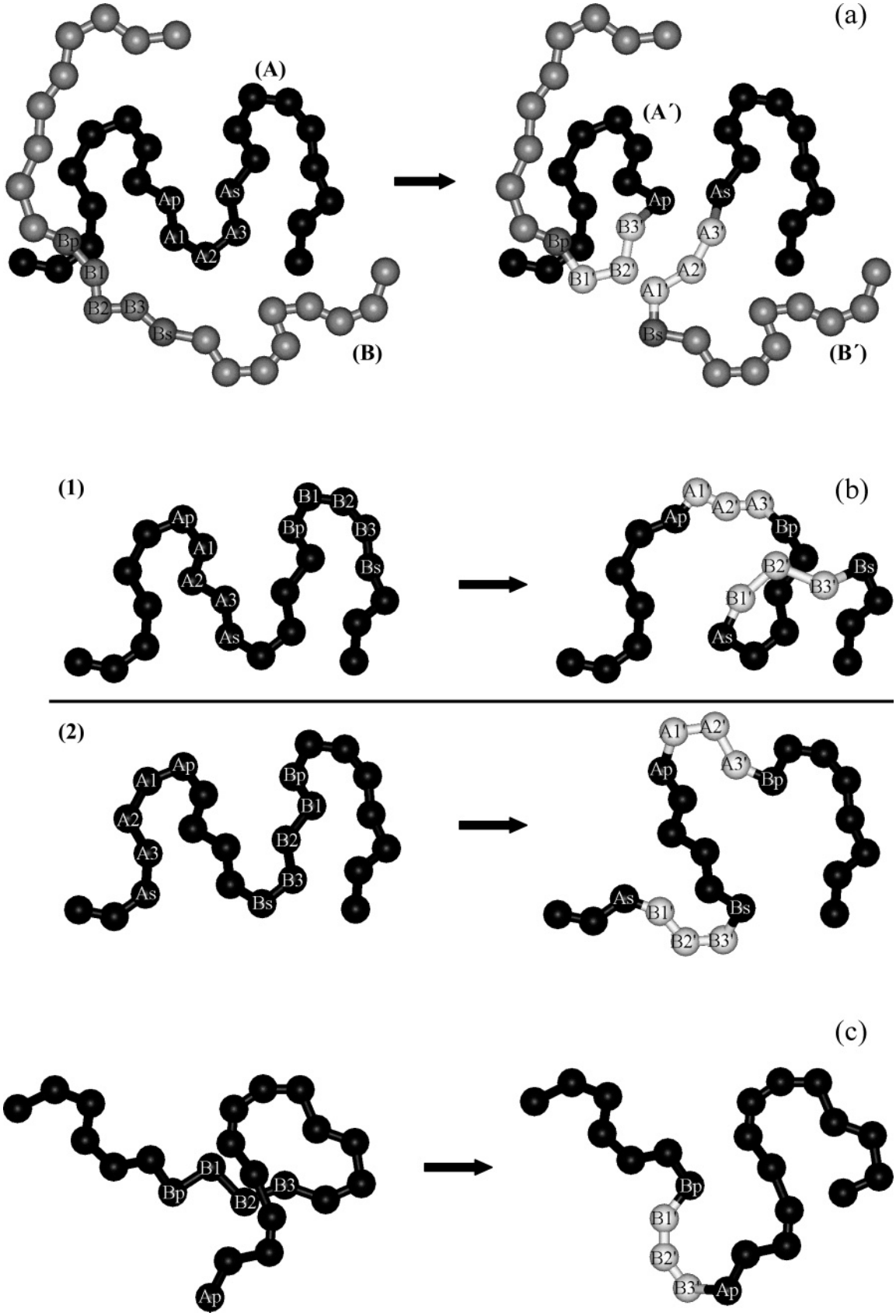

Figure 5. Schematic representation of the chain connectivity altering MC moves employed in the simulations of the longer $CH_3(CH_2)_n-SH/Au(111)$ system of this study: (a) double-bridging (DB); (b) intramolecular double-rebridging (IDR) realized in two ways, (1) and (2); (c) self-end-bridging (SEB).

monodisperse during the simulation, this is the only new configuration considered for acceptance in a trial DB scheme here.

The IDR move is based on the same concepts as the DB move but applies only to a single chain in the system. The IDR move can be realized in two ways, (1) and (2), as depicted in Figure 5b. After proper selection of the two internal atoms (*Ap*, *Bp*), the primary bridging problem is first invoked, permitting atom *Bp* to attack atom *Ap*. The move proceeds by extracting a trimer

of consecutive atoms (*A1*−*A2*−*A3*) adjacent to atom *Ap* and constructing a new trimer (*A1′*−*A2′*−*A3′*) to connect atom *Ap* to atom *Bp*. For completion of the IDR move, a secondary bridging is needed so as to conserve the chain's connectivity and continuity. This secondary bridging is achieved by removing a neighboring-to-*Bp*-atom trimer, namely (*B1*−*B2*−*B3*), and bridging atoms *As* and *Bs* with a new trimer (*B1′*−*B2′*−*B3′*). Note that the selection of atoms *As* and *Bs* is not made at random, but these atoms must be located four bonds away from atoms *Ap* and *Bp*, respectively. It should also be mentioned that the difference between the two possible schemes (1) and (2) of the IDR move is based on the selection of the position of the two trimers relative to atoms *Ap* and *Bp*.

Self-End-Bridging. Like the DB and IDR Monte Carlo moves, the self (i.e., intramolecular)-end-bridging (SEB) move also relies upon the solution of a geometric bridging problem, but its implementation is simpler in the way that only one (the primary) bridging is involved. As it is schematically depicted in Figure 5c, the SEB move is initialized by selecting a chain-end atom *Ap* which is going to attack a properly selected internal atom *Bp* in the same chain. The move proceeds by extracting a trimer adjacent to atom *Bp* lying between atoms *Ap* and *Bp*, namely (*B1*−*B2*−*B3*). To complete the move, a new trimer bridge (*B1′*−*B2′*−*B3′*) must be constructed to connect atoms *Ap* and *Bp* so as to maintain the chain's continuity. From Figure 5c, it is clear that the SEB Monte Carlo move, contrary to the two previously mentioned ones (DB and IDR), alters the identity of chain ends in the sense that an internal atom of a chain becomes an end atom and vice versa.

D. Simulation Methodology: Systems Studied, System Equilibration

The ability of the new MC algorithm based on the set of moves described in section C to fully equilibrate alkanethiol SAMs adsorbed on a Au(111) surface is demonstrated here in the simulation of three different $CH_3-(CH_2)_n-SH$ systems with $n = 9$, 15, and 21, respectively, exposed to a Au(111) surface on the one side (at the bottom) and to a vacuum on the other (at the top), along the *z* direction of an *xyz* coordinate system. The simulation box is orthorhombic with different edge lengths L_x, L_y, and L_z along the *x*, *y*, and *z* directions of the coordinate system; periodic boundary conditions apply only along *x* and *y*. It contains 110 chains, and its dimensions along *x* and *y* are $L_x = 54.67$ Å and $L_y = 43.041$ Å. Using a lattice spacing of 4.97 Å, these values have been calculated to comply with the periodicity of the hexagonal $(\sqrt{3} \times \sqrt{3})R30°$ packing. L_z, on the other hand, has been simply taken to be larger than the thickness of the monolayer at equilibrium.

Our simulation strategy involves the following steps. First, an initial configuration is generated by employing the biased, pseudo-MC approach of the constant density energy-minimization technique of Theodorou and Sutter,[35] accounting also for the presence of the Au(111) surface.[39,50,51] A typical example of the configuration obtained at the end of this first, energy-minimization step with the simulated $CH_3-(CH_2)_9-SH$ system is shown in Figure 6a; it is evident in Figure 6a that, at the end of the energy-minimization step, only a small number (about 40 here) of S atoms have been adsorbed on Au.

In a second step, the configuration obtained at the end of the energy-minimization step is subjected to a long MC simulation in the canonical (NVT) statistical ensemble at a temperature of $T = 300$ K, with the set of moves described in section C. A typical mix of moves employed in this step is as follows: 5% end-mer rotations, 5% flips, 20% concerted rotations, 20% configurational bias, 20% modified bias reptations, and 30% atom-identity exchanges. Their acceptance ratios for the $CH_3-(CH_2)_9-SH$ system are presented in Table 5. Two values for every move are presented in Table 5 corresponding to their acceptance rate before and after the formation of the monolayer. As depicted in Table 5, the modified bias reptation and atom-identity exchange moves, which are predominantly responsible for the adsorption of molecules, exhibit a zero acceptance ratio at full coverage phase, reflecting the difficulty for an alkanethiol molecule to detach from the Au surface and hence the stability of the formed monolayer at $T = 300$ K.

When the Hautman−Klein molecular model was employed in the atomistic simulations, the above mix of moves was found to be efficient enough to drive all S atoms on the Au(111) surface starting from an initial configuration (see, e.g., Figure 6a), leading to the formation of a dense monolayer (as depicted in Figure 6b). This is confirmed in Figure 7a, showing the evolution of the surface coverage with CPU time: within about 2.20×10^8 MC iterations (corresponding to 3 days of computational time), all 110 $CH_3-(CH_2)_9-SH$ chains were adsorbed on the Au(111) surface. Unfortunately, that was not observed to be the case with model II; the higher σ_{ss} value assumed in this model for the S−S interaction did not allow all 110 $CH_3-(CH_2)_9-SH$ to adsorb on the Au(111) plane within the limits of the available CPU time. Figure 7b, for example, shows that after 1×10^9 MC iterations, only 90% of the gold surface's full coverage has been completed. To deal with this, we designed and implemented a parallel version of the MC algorithm, very similar in nature to the parallel tempering method.[52] According to the new work, instead of swapping configurations between different temperatures, we considered an extended ensemble of *n* systems ($i = 1, \ldots, n$) each one of which is a replica of the original system, equilibrated however at a different value of the sulfur−sulfur repulsive core potential ($\sigma_{ss,i}, \ldots, \sigma_{ss,n}$ with $\sigma_{ss,1} > \sigma_{ss,2} > \ldots > \sigma_{ss,n}$) at the same temperature ($T = 300$ K here).

In this parallel Monte Carlo method, besides the MC moves described in part C above, an extra move is introduced, realized by swapping configurations between systems with adjacent sulfur core diameters. The acceptance probability of a swapping move between system configurations *i* and $j = i + 1$ is given by

$$p_{\mathrm{acc}[(i,j)\to(j,i)]} = \min[1, \exp\{-\beta(U^{\mathrm{new}}_{\mathrm{inter}_{ss},i} + U^{\mathrm{new}}_{\mathrm{inter}_{ss},j}) + \beta(U^{\mathrm{old}}_{\mathrm{inter}_{ss},i} + U^{\mathrm{old}}_{\mathrm{inter}_{ss},j})\}] \quad (11)$$

where

$$U^{\mathrm{new}}_{\mathrm{inter}_{ss},i} = \sum_{m=1}^{N-1}\sum_{n=m+1}^{N} 4\epsilon\left[\left(\frac{\sigma_{ss,j}}{r_{mn}}\right)^{12} - \left(\frac{\sigma_{ss,j}}{r_{mn}}\right)^{6}\right]$$

$$U^{\mathrm{old}}_{\mathrm{inter}_{ss},i} = \sum_{m=1}^{N-1}\sum_{n=m+1}^{N} 4\epsilon\left[\left(\frac{\sigma_{ss,i}}{r_{mn}}\right)^{12} - \left(\frac{\sigma_{ss,i}}{r_{mn}}\right)^{6}\right] \quad (12a)$$

and

$$U^{\mathrm{new}}_{\mathrm{inter}_{ss},j} = \sum_{m=1}^{N-1}\sum_{n=m+1}^{N} 4\epsilon\left[\left(\frac{\sigma_{ss,i}}{r_{mn}}\right)^{12} - \left(\frac{\sigma_{ss,i}}{r_{mn}}\right)^{6}\right]$$

$$U^{\mathrm{old}}_{\mathrm{inter}_{ss},j} = \sum_{m=1}^{N-1}\sum_{n=m+1}^{N} 4\epsilon\left[\left(\frac{\sigma_{ss,j}}{r_{mn}}\right)^{12} - \left(\frac{\sigma_{ss,j}}{r_{mn}}\right)^{6}\right] \quad (12b)$$

symbolize the potential intermolecular energy due to S−S interactions after and before the move for the system in configurations *i* and *j*, respectively, with *N* being the total number of S atoms in the system.

In this work, the two $CH_3-(CH_2)_n-SH$ systems were selected to be simultaneously equilibrated at the following 15 different

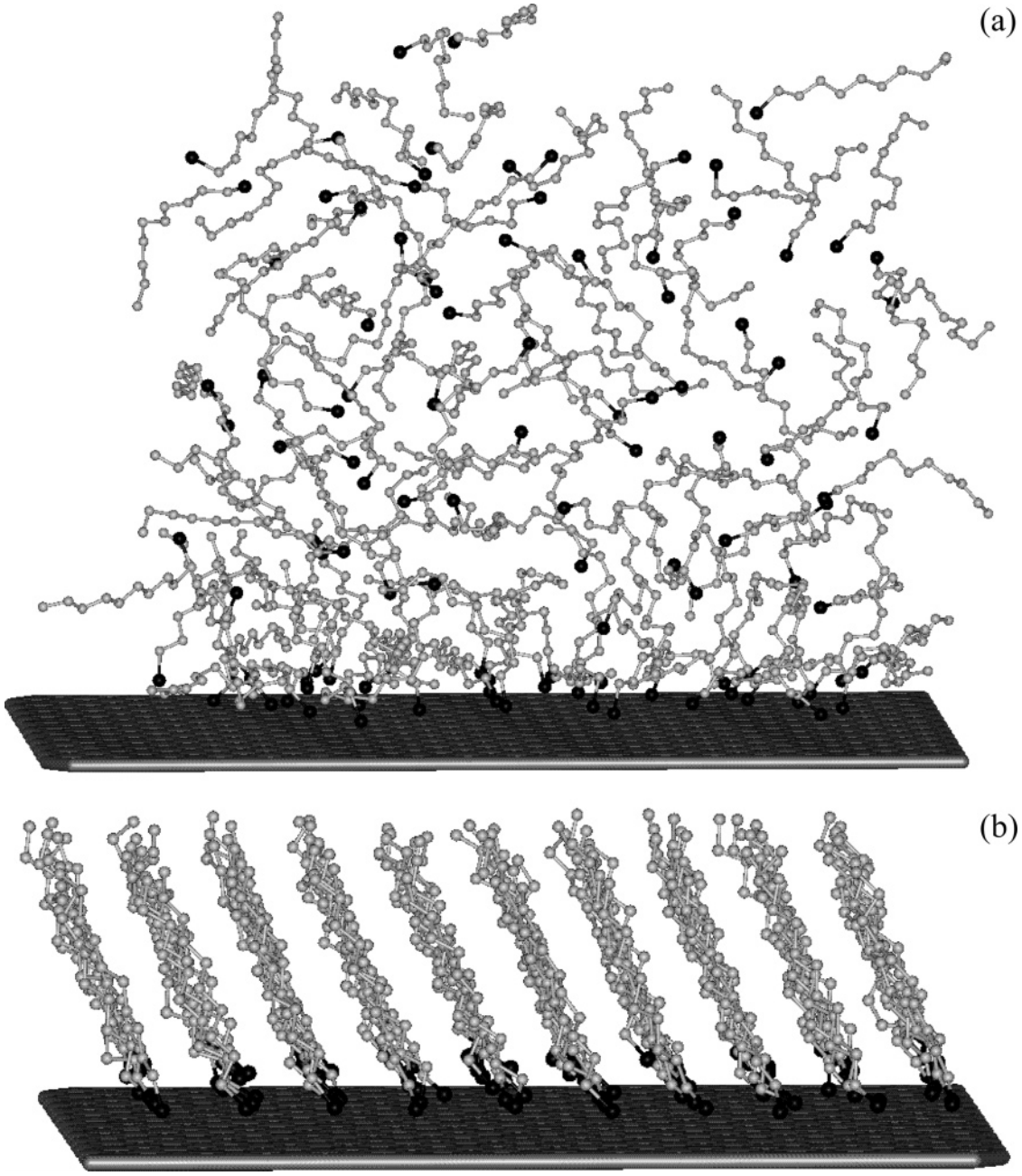

Figure 6. Typical atomistic view of the simulated 110-chain $CH_3(CH_2)_9-SH$/Au(111) system: (a) at the end of the energy-minimization step; (b) at the end of the thermal equilibration with the proposed Monte Carlo algorithm at $T = 300$ K, using the Hautman−Klein molecular model.[17]

TABLE 5: Acceptance Rates of the Monte Carlo Moves Employed in the Present Simulations with the $CH_3(CH_2)_9-SH$ System, before and after Full Coverage on the Au(111) Phase

	$CH_3(CH_2)_9-SH$ acceptance rate (%)	
Monte Carlo moves	before	after
end rotation	9	6
flip	43	47.52
CONROT	1	0.2
CCB	26	25
bias reptation	8	0.015
end atom-identity exchange	11	0

values of σ_{ss}: 4.97, 4.95, 4.93, 4.91, 4.89, 4.87, 4.85, 4.82, 4.79, 4.76, 4.73, 4.69, 4.65, 4.61, and 4.57 Å. MC simulations at each one of them were started from the initial configuration corresponding to the lowest σ_{ss} value (4.25 Å) considered in the serial MC runs. The 15 σ_{ss} values were determined by trial and error so that configurations belonging to neighboring states (different σ_{ss} values) have potential energy histograms that overlap with each other. If this was not the case, the success probability of the attempted swap moves would tend to zero and practically no swapping would occur. Such a criterion imposes a lower limit on the spacing between successive σ_{ss} levels that can be used in the simulation, in order for swapping to be efficient. A histogram reweigthing method was also invoked (reweighted histograms should superimpose; see ref 52 for details) to make sure that the instantaneous potential energy histograms are sampled from configurations corresponding to fully equilibrated systems.

To compare the efficiency of the parallel MC scheme against that of the conventional (serial) MC algorithm, the same configuration was also subjected to serial MC runs for some of the above σ_{ss} values. Through this parallel-σ_{ss} scheme, we were able to equilibrate configurations at such a maximum value of σ_{ss} as the 4.97 Å prescribed by the Siepmann−McDonald model

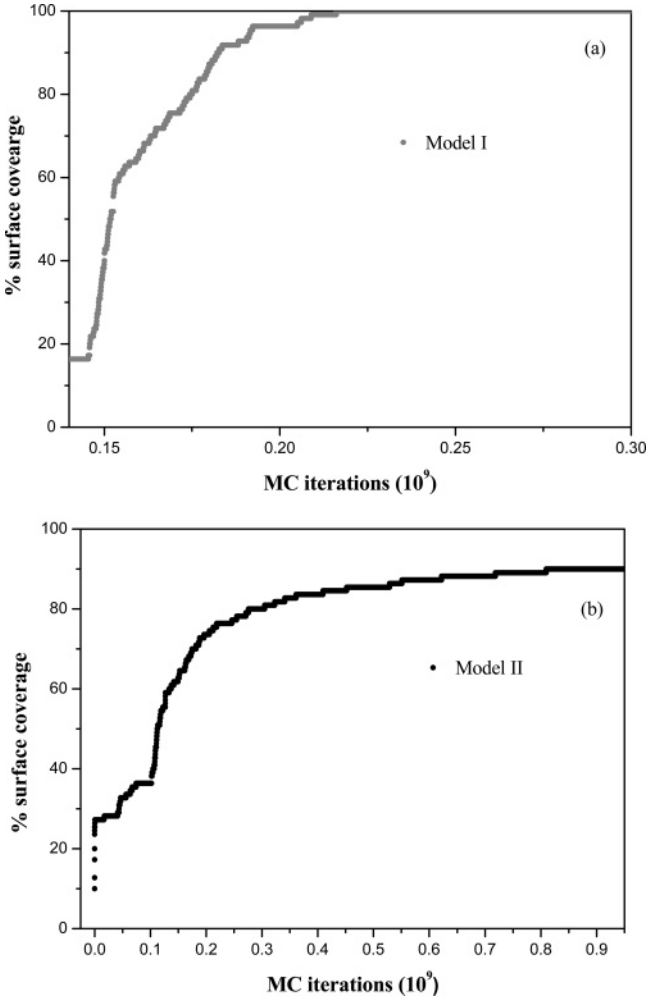

Figure 7. Time evolution of the percentage of $CH_3(CH_2)_9-SH$ chains adsorbed on the Au(111) surface in the course of the atomistic simulation with the new MC algorithm at $T = 300$ K, when the simulation is carried out serially: (a) using the Hautman−Klein[17] molecular model; (b) using the Siepmann−McDonald[19] molecular model.

(model II). This is demonstrated in Figure 8, presenting the time evolution (in MC iterations) of the percentage of $CH_3-(CH_2)_9-SH$ molecules adsorbed on the Au(111) surface in the course of the parallel MC run with model II (starting from the configuration reached at the end of the corresponding serial run characterized by approximately 75% surface coverage). The proposed strategy of simultaneously equilibrating a number of systems with different sulfur core diameter values significantly accelerates chain adsorption for the phase of configurations characterized by higher σ_{ss} values by accepting configurations from the systems characterized by lower σ_{ss} values which are faster in equilibration, leading eventually to the desired full coverage. When all sulfur atoms have been adsorbed on the Au(111) surface (100% surface coverage), the second step is considered as having been completed. A typical system configuration obtained at the end of these parallel MC simulations with model II is shown in Figure 9.

The same strategy was implemented also for the systems of the longer alkanethiol molecules that were equilibrated here with the model proposed by Hautman and Klein.[17] As can be seen in Figure 10 for the $CH_3-(CH_2)_{15}-SH/Au(111)$ system, for example, the higher molecular length employed in the serial execution of the MC algorithm slowed down the adsorption on the gold surface: after 1 billion MC iterations, the surface

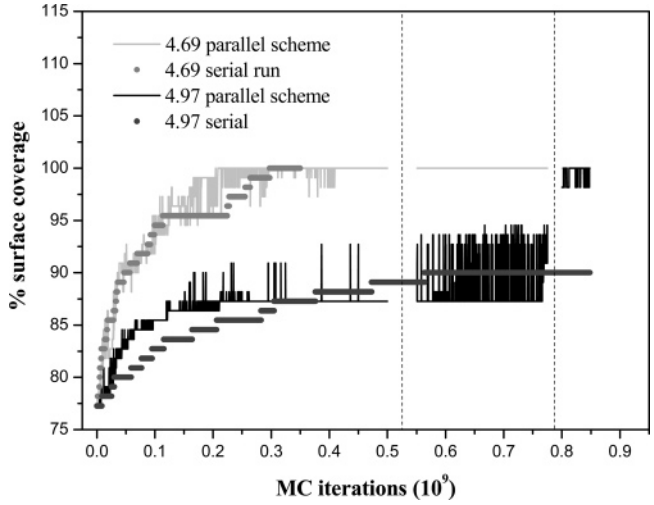

Figure 8. Time evolution of the percentage of $CH_3(CH_2)_9-SH$ chains adsorbed on the Au(111) surface in the course of the atomistic simulation with the new MC algorithm at $T = 300$ K with the Siepmann−McDonald molecular model,[19] when the simulation is carried out in parallel in an extended ensemble of system configurations, each one of which is characterized by a different value of the sulfur−sulfur repulsive core potential parameter, σ_{ss} (from 4.69 to 4.97 Å). By allowing for swaps between configurations corresponding to different σ_{ss} values, the thermal equilibration of the system at the highest σ_{ss} value (the one prescribed by the Siepmann−McDonald molecular model) is significantly accelerated.

coverage reached a plateau at 90% of the gold substrate's full coverage. By employing the strategy of parallel MC execution from that point on, system equilibration was dramatically facilitated in the next billion MC iterations and beyond, leading eventually to full coverage of the $CH_3-(CH_2)_{15}-SH$ SAM on Au(111), as depicted in Figure 11.

In the next (third) and final step, the MC simulation is carried on until all system properties reach the state of thermodynamic equilibrium, that is, until they start fluctuating around a constant average value characteristic of a fully relaxed system. By averaging over a large number of such fully relaxed and statistically uncorrelated configurations, one can extract reliable predictions for all structural properties of the formed R−SH/Au(111) SAM. These include the sulfur−sulfur pair distribution function and the degree of their hexagonal ordering parameter on the Au(111) surface, the mean conformational path along an R−SH chain, the percentage of gauche defects near chain ends, and the distribution of the three angles (tilt, precession, and twist) characterizing chain orientation in the formed monolayer. Representative results for these properties are reported and discussed in the next section (section E) of this paper. A more extended version of section E (including a complete list of figures and a detailed discussion of all simulation findings) is available in the Supporting Information.

E. Results and Discussion

1. The Effect of the Molecular Model. *Mean Conformational Path.* Simulation results for the mean height above the Au(111) surface of all atoms along the chain backbone in the $CH_3-(CH_2)_9-SH/Au(111)$ system (see Supporting Information Figure S1) indicate identical heights for the first five atoms for both models. Starting from the sixth atom on, then, slight differences appear in the *z* coordinates which are seen to become more intense as the terminal methyl group is approached. It is also observed that, independently of the employed molecular model, the averaged *z* distance varies linearly with atom ranking

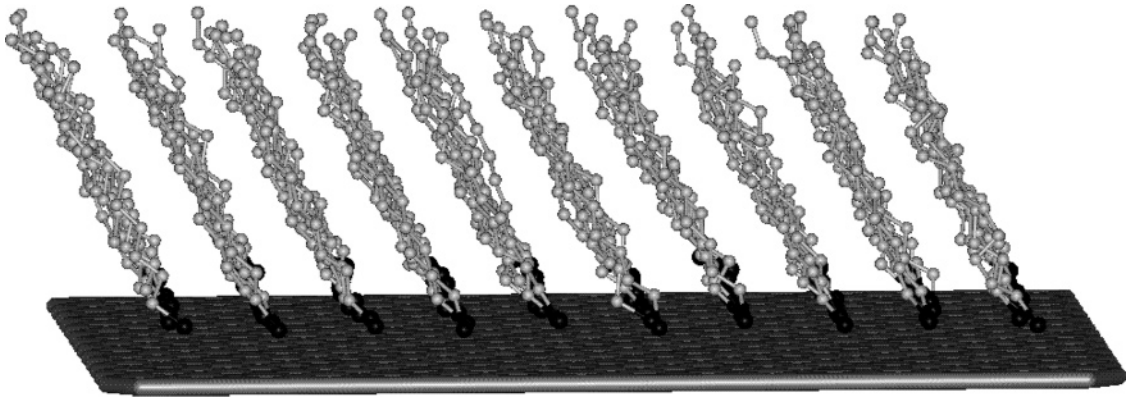

Figure 9. Typical atomistic view of the 110-chain $CH_3(CH_2)_9-SH/Au(111)$ system at the end of the thermal equilibration with the new, parallel-σ_{ss} Monte Carlo code at $T = 300$ K, using the Siepmann−McDonald molecular model.[19]

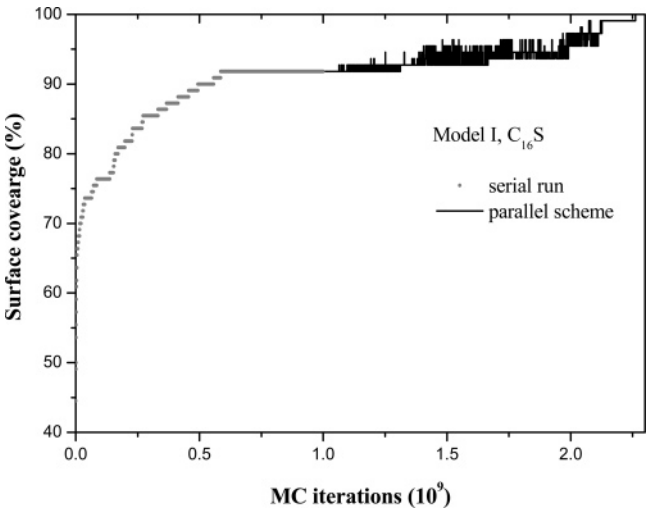

Figure 10. Time evolution of the percentage of $CH_3(CH_2)_{15}-SH$ chains adsorbed on the Au(111) surface in the course of the atomistic simulation with the new Monte Carlo code at $T = 300$ K, using the Hautman−Klein[17] molecular model. Here, the simulation has been executed serially for the first billion and in parallel for the last billion of MC iterations and beyond (by allowing for swaps between system configurations characterized by different σ_{ss} values).

number, implying that chains assume fully extended conformations in the adsorbed monolayer. Numerical values of the average z coordinates of the sulfur headgroups, $\langle z_{head} \rangle$, and methyl tails, $\langle z_{tail} \rangle$, for both models are given in Table 6 (reported errors in the data represent the variance of the mean). For each one of them, the differences between the two models are negligible as far as the $\langle z_{head} \rangle$ values are concerned, but the thicknesses (quantified by the $\langle z_{tail} \rangle$ value) are slightly different: $\langle z_{tail} \rangle$ is larger for model II than for model I by about 0.1 Å. Experimentally, the monolayer thickness is calculated with optical ellipsometry and the values reported for the $CH_3-(CH_2)_9-SH/Au(111)$ system are practically identical to those listed in Table 6 here.[5,9,16]

Molecular Orientation. As discussed in section A, the orientation of an all-trans chain in space can be described by the three Euler angles (tilt, twist, and precession) defined in Figure 1. In Table 6, we list results for the average molecular tilt, $\langle \theta_m \rangle$, for the simulated $C_{10}S/Au(111)$ system. As expected from the corresponding differences in the monolayer thickness, this system tilts less when it is simulated with model II than when it is simulated with model I. This is further clarified in Figure 12, where the normalized distributions of the molecular tilt are compared for the two models, and in Supporting Information Figure S2 illustrating the time evolution (in MC iterations) of the collective molecular tilt. However, the two models are consistent with the experimental data reported in refs 5 and 9 for the simulated $CH_3-(CH_2)_9-SH/Au(111)$ SAM, according to which the average tilt angle should be between 27 and 28°.

Additional simulation data for the direction of the tilt (see Supporting Information Figures S3 and S4) for all chains in the $CH_3-(CH_2)_9-SH/Au(111)$ SAM over the $x-y$ plane prove that the two molecular models exhibit a different behavior: although both display a high degree of homogeneity of the overall tilt direction, a tendency of molecules to tilt toward the nearest neighbor direction is observed in the plots obtained with the Siepmann−McDonald model. The Hautman−Klein model produces a distribution of precession angles with a maximum near 12°, while molecular model II gives a precession angle distribution with a most probable value near 0°. Experimentally,[1] the angle of the tilt direction for the $CH_3-(CH_2)_n-SH/Au(111)$ SAM system with molecular length $n = 9$ is reported to vary between 12 and 15°; it has also been observed[1] that by increasing the molecular length of the chain (e.g., to $n \geq 16$) a transition is observed toward the next nearest neighbor (NNN) arrangement (corresponding to angles of $\chi \sim 30°$).

Gauche Defects along Chain. To determine whether or not the resulting SAM configurations were defect-free or not, we studied the fraction of gauche defects along an alkanethiol chain. Gauche defects (g^- and g^+) were identified by the peaks at the dihedrals around 60 and 300° in the computed distribution(s) of torsion angles in the simulated system(s). We found that (see Supporting Information Figure S5) most of the extra defects occur in the last bond, associated with the extra freedom of the methyl tail group around its axis as compared to interior atoms. In addition, and in agreement with past simulation studies,[17,20] the fraction of gauche defects was observed to oscillate between a smaller and a higher value for every other bond along the chain, an arrangement that helps the chain backbone avoid overlaps with neighboring molecules.

Sulfur Ordering on the Au(111) Surface. In order to elucidate whether or not sulfur atoms exhibit highly ordered structures on the gold surface, we determined the hexagonal order parameter, Ψ_6:[53]

$$\Psi_6 = \left\langle \left| \frac{1}{6n} \sum_{m=1}^{n} \sum_{k=1}^{6} \exp(i6\phi_{mk}) \right|^2 \right\rangle \qquad (13)$$

providing a measure of how closely to the perfectly hexagonal arrangement is the structure of the adsorbed sulfur atoms. For a perfectly hexagonal crystalline phase, $\Psi_6 = 1$, whereas, for completely disordered structures, $\Psi_6 = 0$. The first summation

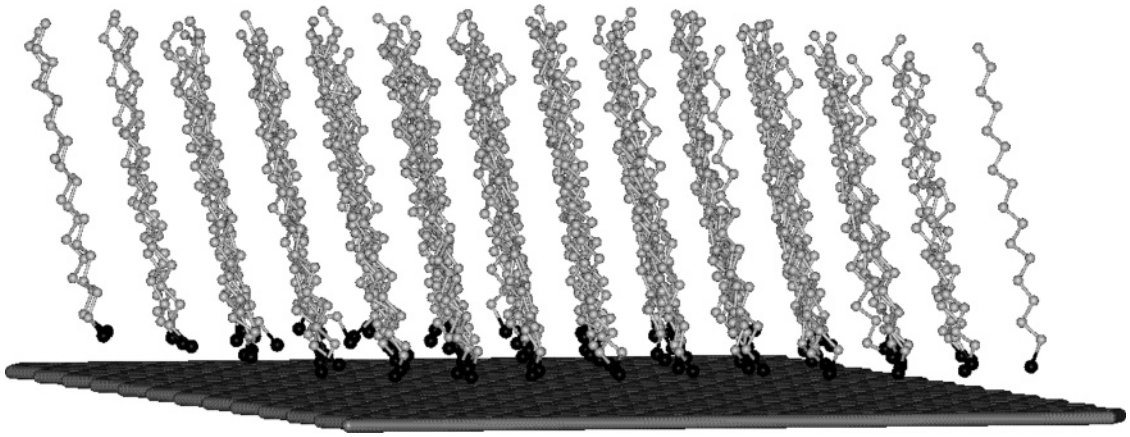

Figure 11. Typical atomistic view of the 110-chain $CH_3(CH_2)_{15}-SH/Au(111)$ system at the end of the thermal equilibration with the new, parallel-σ_{ss} Monte Carlo code at $T = 300$ K, corresponding to the Hautman−Klein[17] molecular model.

TABLE 6: Selected Results from the Monte Carlo Simulations with the $CH_3(CH_2)_9-SH/Au(111)$ System and Their Dependence on the Employed Molecular Model

	$CH_3-(CH_2)_9-SH$	
conformation properties	model I	model II
$\langle z_{head} \rangle$ (Å)	2.41 ± 0.06	2.41 ± 0.06
$\langle z_{tail} \rangle$ (Å)	13.5 ± 0.5	13.6 ± 0.4
$\langle z_{tail} \rangle$ (Å), experimental	12−14[a]	12−14[a]
$\langle \theta_m \rangle$ (deg)	28.6 ± 0.8	27.8 ± 0.7
$\langle \theta_m \rangle$ (deg), experimental	27−28[b]	27−28[b]

[a] Value taken from ref 16. [b] Values taken from refs 5 and 9.

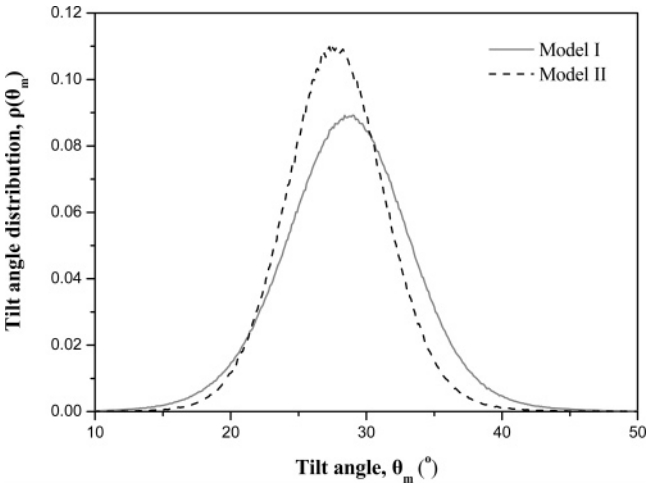

Figure 12. Normalized distributions of the molecular tilt angle in the $CH_3-(CH_2)_9-SH/Au(111)$ system. The dependence of the results on the molecular model is also included.

over m in eq 13 refers to the adsorbed sulfur atoms and the second over k to the six nearest neighbors of m; also, ϕ_{mk} is the angle defined by the vector connecting two headgroups and an arbitrary reference axis (here, the y axis). The results for the simulated $CH_3-(CH_2)_9-SH/Au(111)$ system at $T = 300$ K are depicted in Figure 13. The conclusion drawn from this plot is that the system under study exhibits a higher degree of ordering in the case of model II, which is very close to the hexagonal crystalline phase (Ψ_6 is near 0.88). In contrast, in the structures produced by model I, $\Psi_6 \sim 0.5$, implying the formation of less ordered monolayers far from the perfect hexagonal (but not completely disordered ones).

Figure 14 presents simulation results for the radial pair distribution function, $g(r)$, of the sulfur head groups on the substrate, for the simulated $CH_3-(CH_2)_9-SH/Au(111)$ system.

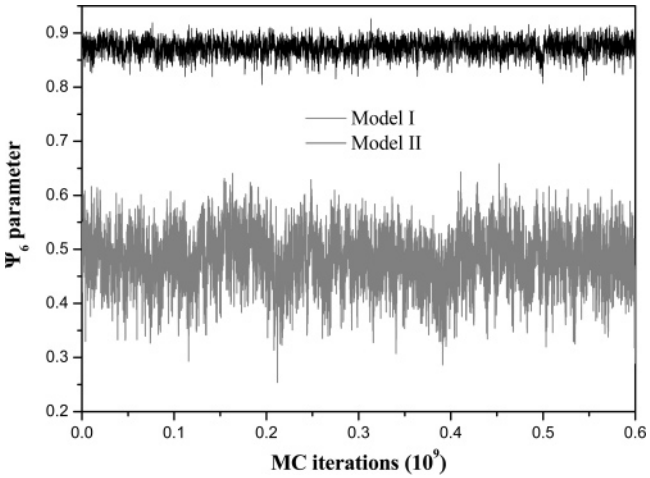

Figure 13. Instantaneous values of the two-dimensional order parameter, Ψ_6, given by eq 13 of the main text, as a function of the number of MC iterations, for the $CH_3-(CH_2)_9-SH/Au(111)$ system (including the dependence on molecular model).

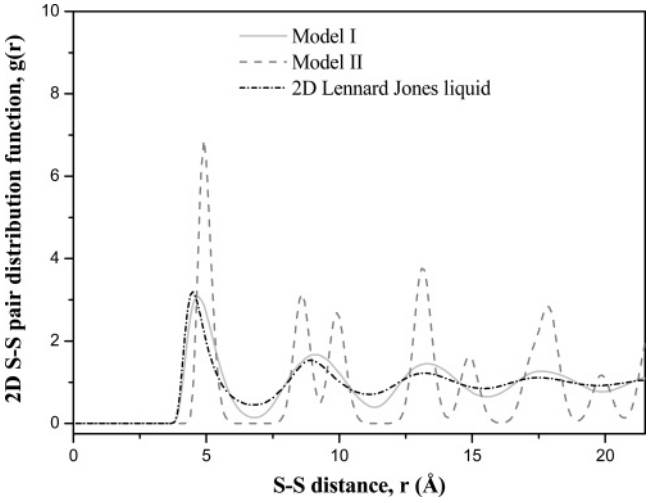

Figure 14. Two-dimensional sulfur−sulfur pair distribution functions on the gold surface.

Also shown in the figure are the results obtained from a corresponding MC simulation with a two-dimensional LJ liquid consisting of the same number of S atoms at the same temperature (300 K) for a value of $\sigma_{ss} = 4.25$ Å. It is concluded again that the Siepmann−McDonald model leads to a more ordered monolayer on the Au(111) surface, comparable to the perfect hexagonal ordering.

TABLE 7: Selected Results from the Monte Carlo Simulations with the $CH_3(CH_2)_n-SH$/Au(111) Systems Using the Molecular Model of Hautman and Klein[17] (The Dependence on the Molecular Length Is Also Included)

	$CH_3-(CH_2)_n-SH$		
conformation properties	$n = 9$	$n = 15$	$n = 21$
$\langle z_{tail} \rangle$ (Å)	13.5 ± 0.5	19.7 ± 0.3	26.2 ± 0.3
$\langle z_{tail} \rangle$ (Å), experimental	12−14	17.5−21.5[a]	25−33[a]
$\langle \theta_m \rangle$ (deg)	28.6 ± 0.8	30.8 ± 0.8	30.7 ± 0.8
$\langle \theta_m \rangle$ (deg), experimental	27−28	30.5−31.5[b]	30.5[b]

[a] Value taken from ref 16. [b] Value taken from ref 1.

An interesting point to make here is the following: Contrary to the simulation results for $\langle z_{tail} \rangle$, $\langle z_{head} \rangle$, and $\langle \theta_m \rangle$ (see Table 6) for which the differences between the two models are rather small, the data of Figures 13 and 14 for Ψ_6 and the ordering of the sulfur groups on the Au(111) plane are different enough so that the present simulations can be used to choose between the two models.

2. The Effect of Chain Length. *Molecular Orientation vs n.* As mentioned above, to elucidate the dependence of the structure of the formed $CH_3-(CH_2)_n-SH$/Au(111) monolayer on the chain length, *n*, of the alkanethiol, MC simulations were performed with three different systems: $C_{10}S$, $C_{16}S$, and $C_{22}S$ on the Au(111) surface using the molecular model of Hautman and Klein, at $T = 300$ K. The results for the dependence of the molecular tilt angle on chain length, *n* (see Supporting Information Figure S6), showed that, contrary to previous theoretical works in the literature,[27] the behavior of the tilt angle does not seem to depend strongly on *n* at least for the regime of molecular lengths considered here: as can be observed at Supporting Information Figure S6 and from the average θ_m values reported in Table 7, when *n* increases from 10 to 16 carbon atoms, the chain tilt increases by about 2° (from 28.6 to 30.8°). A further increase in the molecular length to $n = 22$ carbon atoms leads to an insignificant change of the molecular tilt angle to a value of 30.6° which is within the error limits. It is expected that, for higher molecular lengths ($n > 30$), no tilt structure will be practically observed but this will be the subject of a future investigation.

Additional data for the normalized distributions of the precession angle, χ, in the three SAMs (see Supporting Information Figure S7) demonstrated a transition of the orientation of the three systems from the nearest neighbor (NN) to the next nearest neighbor (NNN) direction with increasing chain length. Indeed, the peaks in the corresponding distribution functions shifted from 12° for the $C_{10}S$ system to 20° for the $C_{16}S$ system and to 30° for the $C_{22}S$ one. This trend has also been observed in experimental measurements.

Gauche Defects vs n. To study the effect of chain length on the percentage of gauche defects along the alkanethiol chain, we also calculated the distribution of torsion angles in the three systems ($C_{10}S$, $C_{16}S$, and $C_{22}S$), and the results obtained are reported in Supporting Information Figure S8. Gauche defects (g^- and g^+) in the figure are represented by the peaks at 60 and 300°. As expected from the analysis of the results referring to the chain length dependence of the molecular tilt, the number of gauche defects was found to be higher for the systems that exhibit a smaller tilt, a phenomenon directly related to the available free volume between side chains. This is demonstrated in Supporting Information Figure S9, showing the percentage of gauche defects as a function of molecular length for all bonds in the three simulated systems ($C_{10}S$, $C_{16}S$, and $C_{22}S$). Indeed, for the $C_{22}S$ system, the fraction of gauche conformations is significantly smaller compared to those in the shorter $C_{10}S$ and $C_{16}S$ systems for all bonds along the chain (except possibly the last two for which the number of gauche defects is zero irrespectively of the chain length).

F. Conclusions

We have presented a novel MC method that solves the problem of the generation of a fully equilibrated initial configuration for systems of self-assembled alkanethiol monolayers on a Au(111) surface. Thanks to the design and implementation of a number of very efficient MC moves, the new method is capable of driving all alkanethiol molecules to the Au(111) substrate starting from an initial, practically random configuration of alkanethiol molecules above the substrate. The efficiency of the new MC algorithm, that can run either serially or in parallel, was proven in simulations with three different $CH_3-(CH_2)_n-SH$/Au(111) systems, with $n = 9$, 15, and 21, by employing the molecular models proposed by Hautman and Klein (model I) and Siepmann and McDonald (model II), respectively.

Our MC simulations at $T = 300$ K showed that both molecular models produce comparable results for the $CH_3-(CH_2)_9-SH$/Au(111) system as far as the molecular orientation of alkanethiol chains is concerned; chains tilt by about 27−28° on average from the gold surface along the nearest neighbor direction. This is consistent with the experimental results reported in the literature.[5,9] The two models, however, differ markedly as far as their predictions for the two-dimensional structure of sulfur atoms on the gold substrate are concerned (as is quantified by the 2D pair distribution function, $g(r)$, on the gold plane or the corresponding Ψ_6 hexagonal order parameter). This deviation should have been expected, since the larger sulfur core diameter value, σ_{ss} (equal to the hexagonal lattice constant 4.97 Å), assumed in model II significantly constrains the motion of sulfur atoms on the gold plane and leads to a 2D structure very close to the perfect hexagonal ordering.

As far as the tilt structure is concerned, this was found to depend only weakly on molecular length.

Additional simulation results for the monolayer thickness (presented in Table 7) were seen to be consistent with experimental results for all three systems. The percentage of bonds in gauche conformations was significantly larger in the case of the shorter $C_{10}S$ system (as compared, for example, to the larger $C_{22}S$ one). In fact, the effect of molecular length on the fraction of gauche defects in the formed monolayers was observed to be stronger for the internal bonds along the adsorbed alkanethiol chains.

Current efforts focus on the investigation of the effect of the nature of the substrate on the structure and conformation of the formed monolayer. To this end, data from ab initio (i.e., first principles) calculations of a methanethiol molecule adsorbed on three different metal surfaces (such as gold, silver, and platinum) are first exploited in order to develop an accurate classical force field for the description of the sulfur−metal interaction. On the basis of this, detailed atomistic simulations are next carried out with the new MC algorithm in order to study the dependence of the resulting SAM structure on the type of metal onto which the monomolecular film is formed.[54] This information is very important for designing SAMs with tailored or predefined structural properties. We are also extending our MC simulations to longer R−SH/Au(111) systems in order to study the transition from the highly ordered SAM structures to the less organized brushlike conformations of end-grafted polymers with increasing *n*.

Acknowledgment. Financial support by the PENED Greek National Programme, Code No. O1EΔ 136, is gratefully acknowledged. The authors would also like to thank Dr. V. A. Harmandaris for very fruitful discussions in the course of the work.

Supporting Information Available: A more extended version of section E of this paper (including a complete list of figures and a detailed discussion of all simulation findings). This material is available free of charge via the Internet at http://pubs.acs.org.

References and Notes

(1) Schreiber, F. *Prog. Surf. Sci.* **2000**, *65*, 151.
(2) Ulman, A. *Chem. Rev.* **1996**, *96*, 1533.
(3) Nuzzo, R. G.; Dubois, L. H.; Allara, D. L. *J. Am. Chem. Soc.* **1990**, *112*, 558.
(4) Nuzzo, R. G.; Korenic, E. M.; Dubois, L. H. *J. Chem. Phys.* **1990**, *93*, 767.
(5) Porter, M. D.; Bright, B. T.; Allara, D. L.; Chidsey, C. E. D. *J. Am. Chem. Soc*. **1987**, *109*, 3559.
(6) Fenter, P.; Eberhardt, A.; Liang, K. S.; Eisenberger, P. *J. Chem. Phys.* **1997**, *106*, 1600.
(7) Strong, L.; Whitesides, G. M. *Langmuir* **1988**, *4*, 546.
(8) Chidsey, C. E. D.; Liu, G.-Y.; Rowntree, P.; Scoles, G. *J. Chem. Phys.* **1989**, *91*, 4421.
(9) Chidsey, C. E. D.; Loiacono, D. N. *Langmuir* **1990**, *6*, 682.
(10) Camillone, N., III; Chidsey, C. E. D.; Liu, G. Y.; Scoles, G. *J. Chem. Phys.* **1993**, *98*, 3503.
(11) Fenter, P.; Eisenberger, P.; Liang, K. S. *Phys. Rev. Lett.* **1993**, *70*, 2447.
(12) Poirier, G. E.; Tarlov, M. J. *Langmuir* **1994**, *10*, 2853.
(13) Delamarche, E.; Michel, B.; Gerber, C.; Anselmetti, D.; Güntherodt, H.-J.; Wolf, H.; Ringsdorf, H. *Langmuir* **1994**, *10*, 2869.
(14) Parikh, A. N.; Allara, D. L. *J. Chem. Phys.* **1992**, *96*, 927.
(15) Fenter, P.; Schreiber, F.; Berman, L.; Scoles, G.; Eisenberger, P.; Bedzyk, M. *Surf. Sci.* **1998**, *412/413*, 213.
(16) Bain, C. D.; Troughton, E. B.; Tao, Y. T.; Evall, J.; Whitesides, G. M.; Nuzzo, R. G. *J. Am. Chem. Soc.* **1989**, *111*, 321.
(17) Hautman, J.; Klein, M. L. *J. Chem. Phys.* **1989**, *91*, 4994.
(18) Hautman, J.; Klein, M. L. *J. Chem. Phys.* **1990**, *93*, 7483.
(19) Siepmann, J. I.; McDonald, I. R. *Langmuir* **1993**, *9*, 2351.
(20) Mar, W.; Klein, M. L. *Langmuir* **1994**, *10*, 188.
(21) Pertsin, A. J.; Grunze, M. *Langmuir* **1994**, *10*, 3668.
(22) Bhatia, R.; Garrison, B. J. *Langmuir* **1997**, *13*, 765.
(23) Bhatia, R.; Garrison, B. J. *Langmuir* **1997**, *13*, 4038.
(24) Li, T. W.; Chao, I.; Tao, Y. T. *J. Phys. Chem. B* **1998**, *102*, 2935.
(25) Shevade, A. V.; Zhou, J.; Zin, M. T.; Jiang, S. *Langmuir* **2001**, *17*, 7566.
(26) Jiang, S. *Mol. Phys.* **2002**, *100*, 2261.
(27) Vemparala, S.; Karki, B. B.; Kalia, R. K.; Nakano, A.; Vashishta, P. *J. Chem. Phys.* **2004**, *121*, 4323.
(28) Sellers, H.; Ulman, A.; Shnidman, Y.; Eilers, J. E. *J. Am. Chem. Soc.* **1993**, *115*, 9389.
(29) Beardmore, K. M.; Kress, J. D.; Gronbech-Jensen, N.; Bishop, A. R. *Chem. Phys. Lett.* **1998**, *286*, 40.
(30) Yourdshahyan, Y.; Rappe, A. M. *J. Chem. Phys.* **2002**, *117*, 825.
(31) Zhang, L.; Goddard, W. A., III; Jiang, S. *J. Chem. Phys.* **2002**, *117*, 7342.
(32) Fischer, D.; Curioni, A.; Andreoni, W. *Langmuir* **2003**, *19*, 3567.
(33) Jorgensen, W. L. *J. Phys. Chem.* **1986**, *90*, 6379.
(34) Ryckaert, J. P.; Bellemans, A. *Chem. Phys. Let.* **1975**, *30*, 123.
(35) Theodorou, D. N.; Suter, U. W. *Macromolecules* **1985**, *18*, 1467.
(36) Pant, P. V. K.; Theodorou, D. N. *Macromolecules* **1995**, *28*, 7224.
(37) Mavrantzas, V. G.; Theodorou, D. N. *Macromolecules* **1998**, *31*, 6310.
(38) Mavrantzas, V. G.; Boone, T. D.; Zervopoulou, E.; Theodorou, D. N. *Macromolecules* **1999**, *32*, 5072.
(39) Daoulas, K. C.; Terzis, A. F.; Mavrantzas, V. G. *J. Chem. Phys.* **2002**, *116*, 11028.
(40) Vacatello, M.; Avitabile, G.; Gorradini, P.; Tuzi, A. *J. Chem. Phys.* **1980**, *73*, 548.
(41) Boyd, R. H. *Macromolecules* **1989**, *22*, 2477.
(42) Rosenbluth, M. N.; Rosenbluth, A. W. *J. Chem. Phys.* **1955**, *23*, 356.
(43) De Pablo, J. J.; Laso, M.; Suter, U. W. *J. Chem. Phys.* **1992**, *96*, 2395.
(44) Siepmann, I. J.; Frenkel, D. *Mol. Phys.* **1992**, *75*, 59.
(45) Leontidis, E.; De Pablo, J. J.; Laso, M.; Suter, U. W. *Adv. Polym. Sci.* **1994**, *116*, 283.
(46) Zervopoulou, E. I. Ph.D. Dissertation, Department of Chemical Engineering, University of Patras, Greece, 2000.
(47) Dodd, L. R.; Boone, T. D.; Theodorou, D. N. *Mol. Phys.* **1993**, *78*, 961.
(48) Karayiannis, N. C.; Mavrantzas, V. G.; Theodorou, D. N. *Phys. Rev. Lett.* **2001**, *88*, 105503.
(49) Karayiannis, N. C.; Gianousaki, A.; Mavrantzas, V. G.; Theodorou, D. N. *J. Chem. Phys.* **2001**, *117*, 5465.
(50) Mansfield, K. F.; Theodorou, D. N. *Macromolecules* **1990**, *23*, 4430.
(51) Mansfield, K. F.; Theodorou, D. N. *Macromolecules* **1991**, *24*, 4295.
(52) Doxastakis, M.; Mavrantzas, V. G.; Theodorou, D. N. *J. Chem. Phys.* **2001**, *115*, 11352.
(53) Stadler, C.; Lange, H.; Schmid, F. *Phys. Rev. E* **1999**, *59*, 4248.
(54) Alexiadis, O.; Harmandaris, V. A.; Mavrantzas, V. G.; Delle Sitte, L. *J. Phys. Chem. C* **2007**, *111*, 6380.